Cleaner Engineering and Technology 4 (2021) 100176

Contents lists available at ScienceDirect

Cleaner Engineering and Technology

journal homepage: www.sciencedirect.com/journal/cleaner-engineering-and-technology

Development of ECO-UHPC utilizing gold mine tailings as quartz sand alternative

Tanvir Ahmed [a], Mohamed Elchalakani [a], Hakan Basarir [b], Ali Karrech [a], Ehsan Sadrossadat [a], Bo Yang [c,d,*]

[a] Department of Civil, Environmental and Mining Engineering, Faculty of Engineering, Computing and Mathematical Sciences, The University of Western Australia, 35 Stirling Highway, Crawley, WA, 6009, Australia
[b] Department of Geoscience and Petroleum, Norwegian University of Science and Technology, NO-7491, Trondheim, Norway
[c] Key Laboratory of New Technology for Construction of Cities in Mountain Area, Chongqing University, Chongqing, 400045, China
[d] School of Civil Engineering, Chongqing University, Chongqing, 400045, China

ARTICLE INFO

Keywords:
CO_2
Cost
Durability
Mine waste
Sustainability
Ultra-high performance concrete

ABSTRACT

To ensure ultra-high performance, in terms strength and durability, coarse aggregate is typically avoided in UHPC (ultra-high performance concrete). Instead, very fine quartz sand is usually used as the only aggregate. However, excessive extraction of sand from natural resources and its grinding and refining processes to prepare very fine quartz-rich sand are not economically or environmentally lucrative. Limited number of studies sought to address this concern, and very few of these studies investigated the use of mine tailings (quartz based tailings and iron ore tailings) in UHPC as sand alternatives. In the present study, the possibility of utilizing gold mine tailings, sourced from a gold mine in Western Australia (WA), as conventional quartz sand substitute in UHPC has been investigated. Results suggest that UHPCs, made with up to 80% replacement of quartz sand by the tailings, exhibit compressive strengths comparable to or higher than that of the UHPC with 100% quartz sand. 28-day strength greater than 120 MPa is achievable up to 100% replacement. The water absorptions and the initial rate of absorptions of UHPCs with tailings are generally lower than those of the UHPC without tailings. The leachability of toxic metals from UHPC with up to 100% tailings content lies well below the regulatory thresholds. The combined material and transportation cost of UHPC can be reduced by up to 33.1% replacing quartz sand by the tailings, for construction near the mine site. The CO_2 emission can be reduced by up to 12.1%. In the area near the mine site, utilization of the tailings can economically and environmentally, as well as in terms of durability, be a better option than quartz sand for construction works that require UHPC with 28-strength in excess of 120 MPa.

1. Introduction

Compared to normal-strength concrete (NSC) or high-strength concrete (HSC), ultra-high performance concrete (UHPC) exhibits extraordinary mechanical and durability performances. NSC exhibits compressive strength in the range of 20–40 MPa. HSC can achieve strength greater than 40 MPa but seldom greater than 100 MPa. Whereas UHPC, according to a group of researchers, must exhibit a compressive strength greater than 120 MPa (Huang et al., 2019), or greater than 150 MPa according to others (Courtial et al., 2013). The water absorption of NSC is much higher than 3.5% (Neville, 2011), and the absorption of HSC is usually in the range of 1.5%–3% (Nematollahi et al., 2011). The water absorption of UHPC, on the other hand, is typically less than 1.5% (Scheydt and Müller, 2012).

Although UHPC exhibits outstanding mechanical and durability performances, the material cost of UHPC is usually high compared with NSC or HSC. Total exclusion of coarse aggregate and use of only very fine high-quality quartz sand (maximum size $\leq$ 600 μm, quartz content $\geq$ 95%) is one of the factors contributing to its high cost. This is because the extraction, grinding, and refining processes of such fine and high-quality aggregate are energy-intensive and expensive. Extraction and grinding of quartz sand are also associated with several negative environmental consequences. For instance, CO_2 emission, deforestation, loss of biodiversity, soil degradation, lowering of water table, particulate

* Ccorresponding author. Key Laboratory of New Technology for Construction of Cities in Mountain Area, Chongqing University, Chongqing, 400045, China.
E-mail address: yang0206@cqu.edu.cn (B. Yang).

https://doi.org/10.1016/j.clet.2021.100176
Received 16 November 2020; Received in revised form 8 June 2021; Accepted 11 June 2021
Available online 16 June 2021

matter air pollution, etc. (Gavriletea, 2017). According to the United Nations Environment Programme (UNEP), the global sand extraction rate is currently substantially higher than its natural replenishment rate, as sand and gravel are the second most consumed natural resources after water (UNEP, 2014). The global consumption of sand and gravel is approximately 32–50 billion tonnes per year (Bendixen et al., 2019). A number of studies were carried out to investigate the influences of different by-product or waste based alternatives to conventional quartz sand on the properties of UHPC. Jiao et al. (2020) used waste-glass sand to produce UHPC. The 28-day compressive strength of the UHPC with waste-glass sand was observed to increase by around 25% with respect that of the UHPC with quartz sand. Yang et al. (2020) fully substituted quartz sand by recycled rock dust to produce UHPC and observed an increase of 9.5% in the compressive strength. Zhang et al. (2018) used recycled fine aggregate from demolished concrete in UHPC and the strength was found to decrease by 13.3% with respect to that of the control.

In addition to the foregoing types of alternative aggregate, mine tailings (by-products of mineral extraction processes) can potentially be used as aggregates for UHPC production. The mining industry was estimated to produce around 14 billion tonnes of tailings annually, and the amount is increasing because of the increasing use of low-grade ores to meet the global demand for valuable metals (Kinnunen et al., 2018). Mine tailings are usually very fine (especially the ones from mines of precious minerals like gold), due to the grinding of ore into fine particles to extract the target metal (Dong et al., 2019). Because of this, quartz based mine tailings have the potential to be utilized as aggregates and in some cases as supplementary binders in UHPC without the requirement of further grinding. Mine tailings often contain toxic heavy metals. The dense micro-structure of UHPC is, however, supposed to restrict the heavy metals from being leached out of the concrete (Pyo et al., 2018). The use of tailings in UHPC may also address a number of concerns. For instance, the hazards associated with the mismanagement of tailings can be reduced (e.g., workers' safety risk, chemical and toxic metal pollution, etc.), CO_2 emission associated with the extraction and grinding of quartz sand can be decreased, natural sources of quartz sand can be saved from being depleted to some extent, etc. (Ince, 2019).

As can be seen from Table 1, a number of studies were conducted to investigate the influence of utilizing different types of tailings, as sand substitutes, on the properties of NSC and HSC. Few studies can be found in the literature which investigated the possibility of utilizing mine tailings to substitute sand in UHPC. Zhao et al. (2014) and Zhu et al. (2015) investigated the influence of replacing sand by iron ore tailings on the properties of UHPC. The researchers concluded that full substitution of sand by iron ore tailings reduces the strength of UHPC. However, Zhao et al. (2014) observed that up to 20% replacement, the 28-day strength of UHPC remained comparable to that of the UHPC without iron ore tailings. Pyo et al. (2018) used a type of quartz-based mine tailings to partially replace (30% by mass) quartz sand in UHPC, and obtained strength comparable to that of the UHPC with 100% quartz sand. Research addressing the influence of utilizing gold mine tailings, as quartz sand alternative, on the properties of UHPC is scarce in the literature.

In the present study, the possibility of using a type of gold mine tailings as aggregate in UHPC was investigated. UHPC mixes were prepared, replacing quartz sand by the tailings at different percentages (up to 100% by mass). Mechanical properties such as compressive strength, elastic modulus, splitting tensile strength, and durability properties such as water absorption, initial rate of water absorption, carbonation resistance were investigated for the prepared mixes. Leaching toxicity test was conducted for each UHPC mix, to assess the leachability of the heavy metals present in the tailings from the UHPC. Scanning electron microscopy (SEM) was performed for selected UHPC mixes to understand their macro-behaviours. Economic and ecological influences of using the tailings in UHPC, as replacement of conventional quartz sand, were also examined.

2. Materials and methods

2.1. Materials

The gold mine tailings used in this study were sourced from a gold mine site in Western Australia (WA). Due to a confidentiality agreement, the exact location of the mine is not mentioned in the paper. The mine will be termed as Mine 1 in the following discussion. Mining operation in Mine 1 consists of open pit and underground mining. The ore processing plant includes two process trains. Process routes include crushing, milling, flotation, and cyanide leaching. Flotation tailings are thickened. The cyanide in the tailings is recovered and recycled, and a WAD (weak acid dissociable) cyanide level of less than 50 ppm is maintained before discharging the tailings into the tailings storage facility. Further degradation of the remaining cyanide is facilitated through sunlight exposure (Logsdon et al., 1999). For this study, two tonnes of tailings exposed to sun-drying for more than three years were harvested from an old storage area. In the following discussion, the tailings will be termed as WAGT1 (**W**estern **A**ustralian **G**old mine **T**ailings sourced from Mine **1**). The composition of major elements in WAGT1, in terms of oxides, are presented in Table 2. Table 2 also shows the concentrations of several heavy elements (e.g., As, Pb, Zn, Cd, Cr, and Cu) in WAGT1. The chemical properties presented in Table 2 are based on elemental concentrations measured using inductively coupled plasma - optical emission spectrometry (ICP-OES).

The cyanide concentration in the as-received WAGT1 was not measured in the current study. However, the mining company, in charge of WAGT1 management in Mine 1, is a signatory to the International Cyanide Management Code; and it was confirmed by the company that the cyanide concentration in the as-received WAGT1 was well below the hazard level. Detailed investigation on the possibility of acid generation from the sulphide minerals in WAGT1 was not conducted in the present study. However, pH was measured for a mixture of 1 L of deionized water and 60 g of as-received WAGT1. The mixture was stirred for half an hour before measuring the pH. The pH of the mixture was found to be 9.37. The pH value indicates that the as-received WAGT1 were not acidic.

Fig. 1 shows the scanning electron micrograph of WAGT1. Fig. 1 also presents the X-ray diffraction (XRD) pattern of WAGT1 in the 2θ range of 5–70°, recorded using a diffractometer with Cu K radiation ($\lambda = 1.5404$ Å), 40 kV, and 40 mA at a rate of 2°/min. Quartz was found to be the main crystalline phase from the XRD pattern of WAGT1. Peaks corresponding to several other minerals like muscovite, albite, halite, and polyhalite were also observed in their XRD pattern. It is worth noting that these minerals are softer than quartz. On Mohs scale, quartz's hardness is 7. Mohs hardness is in the range of 2–2.5 for muscovite, 6–6.5 for albite, 2–2.5 for halite, and 2.5–3.5 for polyhalite.

The cement used in this study conforms to the requirements of ASTM C150/C150M-16 Type I Portland cement (ASTM C150/C150M-16, 2016), silica fume conforms to AS/NZS 3582.3 amorphous silica (AS/NZS 3582.3, 2016), and fly ash conforms to ASTM C618-19 Class-F fly ash (ASTM C618-19, 2019). The quartz sand had a median diameter (d_{50}) of 237.3 μm and an absorption capacity of 0.38%. The chemical and physical properties of the cement, silica fume, fly ash, and quartz sand are presented in Table 2. It can be seen from Table 2 that the SiO_2 content of the quartz sand was 99.8% and the SiO_2 content of WAGT1 was 71.2%. This indicates that the quartz sand had higher quartz content than that in WAGT1. Fig. 2 shows the particle size distributions (PSD) of all the solid materials. A polycarboxylate based high-range water reducer (HRWR) with 36% solid content and a defoaming agent with 5.5% solid content were used as chemical admixtures.

2.2. Mix proportions

The mix proportions of the prepared UHPC mixes are summarized in Table 3. Quartz sand was used as the aggregate in the control mix T0.

Table 1
A review of mechanical properties of standard-cured[a] structural concretes/mortars incorporating different types of tailings as sand alternatives.

Concrete type	Reference	Tailings		Material replaced	Replacement, %	*w/b*	Replacement at maximum $f_{c,28\text{-}d}$, %	$f_{c,28\text{-}d}$, MPa		
		Location	Type					Maximum	At 0% replacement ($f_{c0,28\text{-}d}$)	At maximum replacement
UHPC ($f_{c0,28\text{-}d} \geq 120$ MPa)	Pyo et al. (2018)	Sang-dong mine, South Korea	Quartz based tailings	Quartz sand	0, 15, 30	0.17	15, 30	133[b]	132[b]	133[b]
	Zhu et al. (2015)	China	Iron ore tailings	Quartz sand	0, 100	0.16	0	189[c]	189[c]	183[c]
				River sand	0, 100		100	183[c]	172[c]	183[c]
	Zhao et al. (2014)	China	Iron ore tailings	River sand	0, 10, 20, 30, 40, 50, 100	0.16–0.20	20	139.2	138	97.2
VHSC/VHSM (100 MPa $\leq f_{c0,28\text{-}d} <$ 120 MPa)	Zhang et al. (2020a)	Liaoning, China	Iron ore tailings	Manufactured sand	0, 20, 40, 60, 80, 100	0.18	40	120	105	95
HSC/HSM (40 MPa $\leq f_{c0,28\text{-}d} <$ 100 MPa)	Gao et al. (2020)	Shangluo, Shaanxi, China	Molybdenum tailings	Sand	0, 25, 50, 100	0.42	0	55	55	48
						0.31	0	61.5	61.5	55.5
	Li et al. (2020)	Yaogou pond, Shaanxi, China	Iron ore tailings	River sand	0, 10, 20, 30, 40, 50, 70, 100	0.40	30	52.2	42	37.5
	Zhang et al. (2020b)	Daye, Hubei, China	Copper tailings	Manufactured sand	0, 20	0.32	0	59	59	57
	Zhang et al. (2020c)	Shangluo, Shaanxi, China	Iron ore tailings	River sand	0, 100	0.35	100	62.4	60.4	62.4
	Xu et al. (2018)	China	Kaolin tailings	River sand	0, 20, 40, 60, 80, 100	0.50	60	58.6	57.5	52.8
NSC/NSM (20 MPa $\leq f_{c0,28\text{-}d} <$ 40 MPa)	Protasio et al. (2021)	Germano dam, Minas Gerais, Brazil	Iron ore tailings	Quartz sand	0, 10, 20, 30	0.55	10	40.9	34.5	39.8
	Liu et al. (2020a)	China	Graphite tailings	River sand	0, 10, 20, 30, 40, 50, 60, 70, 80, 90, 100	0.52	10	42.2	36.9	28
	Fisonga (2019)	Mindolo dam, Copperbelt, Zambia	Copper tailings	Sand	0, 30, 50, 70, 100	0.48–0.53	30	35.6	33.8	25
	Ince (2019)	Lefke-Xeros, Cyprus	Gold mine tailings	Sand	0, 10, 20, 30	0.62	30	42	32.5	41.5
	Kathirvel et al. (2018)	Tamil Nadu, India	Graphite ore tailings	River sand	0, 10, 20, 30, 40, 50, 60, 70, 80, 90, 100	0.50	10	33.2	32.5	14.5
						0.55	10	27	26.3	8
			Treated graphite ore tailings	River sand	0, 10, 20, 30, 40, 50, 60, 70, 80, 90, 100	0.50	10	34.5	32.5	20.5
						0.55	10	28	26.3	14.2
	Gupta et al. (2017)	Khetri, Rajasthan, India	Copper tailings	River sand	0, 10, 20, 30, 40, 50, 60, 70	0.48–0.50	20	31.9	30.9	23.6
	Shettima et al. (2016)	Johor, Malaysia	Iron ore tailings	River sand	0, 25, 50, 75, 100	0.50	25	42.9	38.0	38.5
	Tian et al. (2016)	Zibo, China	Iron ore tailings	River sand	0, 25, 35, 45	0.55	35	39.5	38.7	36.8
	Thomas et al. (2013)	Khetri, Rajasthan, India	Copper tailings	River sand	0, 10, 20, 30, 40, 50, 60	0.40	10	41.5	35	36.5
						0.45	20	39	37.5	33
						0.50	30	37	31.5	32.5

UHPC = ultra-high performance concrete/composite, VHSC/VHSM = very-high-strength concrete/mortar, HSC/HSM = high-strength concrete/mortar, NSC/NSM = normal-strength concrete/mortar, $f_{c0,28\text{-}d}$ = 28-day compressive strength of control mix (mix with 0% tailings), $f_{c,28\text{-}d}$ = 28-day compressive strength, *w/b* = water to binder ratio

[a] Cured in water or in fog room at a relative humidity of 95% ± 5%, and at a temperature of 24 °C ± 6 °C.
[b] Air cured.
[c] Cured in hot water at 100 °C on second and third days.

Table 2
Chemical and physical properties of solid materials.

Material		WAGT1	Sand	Cement	Silica fume	Fly ash
Major elements (mass% of oxide)	Al_2O_3	9.36	0.017	3.18	0.13	23.93
	CaO	2.48	0.002	64.48	0.33	6.98
	Fe_2O_3	4.94	0.008	4.34	0.07	7.94
	K_2O	1.62	0.003	0.35	0.54	1.02
	MgO	1.23	0.003	1.46	0.71	1.27
	MnO	0.079	0.001	0.120	0.008	0.104
	Na_2O	2.22	0.003	0.14	0.29	0.38
	P_2O_5	0.058	0.00	0.228	0.129	0.535
	SiO_2	71.2	99.88	21.4	94.6	55.9
	SO_3	1.89[a]	0.00	2.93	0.07	0.30
	TiO_2	0.494	0.025	0.192	0.005	1.312
	Loss on ignition	4.06	0.05	1.15	3.1	1.71
Heavy elements in WAGT1 (mg/kg)	Zn	151				
	Cd	0.9				
	As	232				
	Pb	12				
	Cu	397				
d_{50} (μm)		141.4	237.3	17.3	1.7	9.8
Specific gravity[b]		2.7	2.65	3.18	2.15	2.38

d_{50} = median diameter

[a] Sulphur (S) content in WAGT1 = 0.76%.
[b] As per manufacturer.

20% of the quartz sand was replaced by WAGT1 (by mass) to prepare T20, 40% was replaced to prepare T40, 60% was replaced to prepare T60, and 100% was replaced to prepare T100. The water to binder ratio (w/b) of the mixes was kept constant at 0.182.

The combined PSD of the solid constituents of each mix is shown in Fig. 3. The target combined PSD [modified Andreasen and Andersen (A&A) model (Eq. (1))] is also shown in Fig. 3. The value of q in Eq. (1) was selected to be 0.22, as suggested by previous studies for mixes with high powder content (<250 μm) (Kim et al., 2016).

$$p(D) = \frac{D^q - D_{min}{}^q}{D_{max}{}^q - D_{min}{}^q} \quad (1)$$

D represents particle size (μm), $p(D)$ is cumulative percent finer than size D, $D_{\min}$ is the minimum size of particle (μm), and $D_{\max}$ is the maximum size of particle (μm).

The root-mean-square error (*RMSE*) and determination coefficient (R^2) between the target PSD curve and each combined PSD curve are presented in Fig. 3. It can be seen that the *RMSE*s between the combined PSDs of the mixes with WAGT1 and the target PSD were lower than that between the combined PSD of T0 and the target PSD. This indicates better particle packing was achieved when WAGT1 were incorporated. The lowest *RMSE* was observed for T60.

2.3. Specimen preparation

For the preparation of each UHPC mix, dry constituents such as cement, silica fume, fly ash, quartz sand, and/or WAGT1 were mixed using a mixer for 3 min. After that, water, HRWR, and defoaming agent were added to the dry mixture and mixed until the mixture became flowable. 50 × 50 × 50 mm cube moulds were used to prepare the specimens for compressive strength tests, 50 × 100 mm cylindrical moulds for splitting tensile strength tests, and 100 × 100 × 100 mm cube moulds for durability tests. The moulded specimens were vibrated for 1 min and then moved to a humidity- and temperature-controlled curing room (95% relative humidity, 21 °C temperature). The specimens were demoulded after 24 h. The mechanical test specimens were fully submerged in water (21 °C) until the time of testing, while the durability specimens were left inside the humidity-controlled curing room. After 28 days, the carbonation test specimens were kept in a CO_2-controlled chamber (60% relative humidity, 21 °C temperature) at an elevated CO_2 concentration of 10,000 ppm for 56 days.

2.4. Test methods

2.4.1. Fresh properties

Slump flow tests were conducted for the fresh UHPC mixes in accordance with AS 1012.3.5 (2015). A mini slump cone, having a height of 116 mm, a top diameter of 38 mm, and a bottom diameter of 76 mm, was used for the slump flow tests. The aspect ratio of the cone was identical to that of the standard cone specified by AS 1012.3.5 (2015).

Wet packing density was measured for each fresh UHPC mix based on the calculation method presented in (Wong and Kwan, 2008). Wet

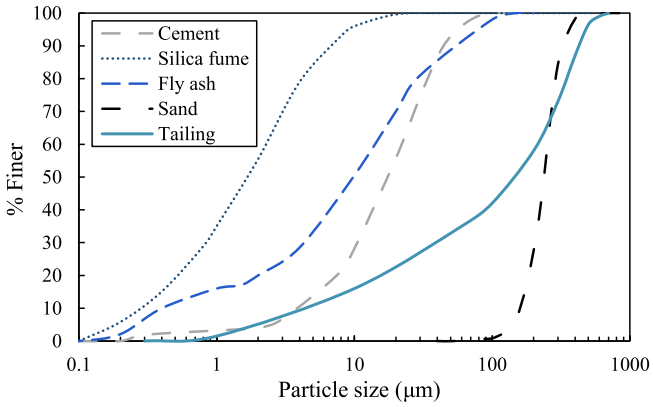

Fig. 2. Particle size distributions of solid materials.

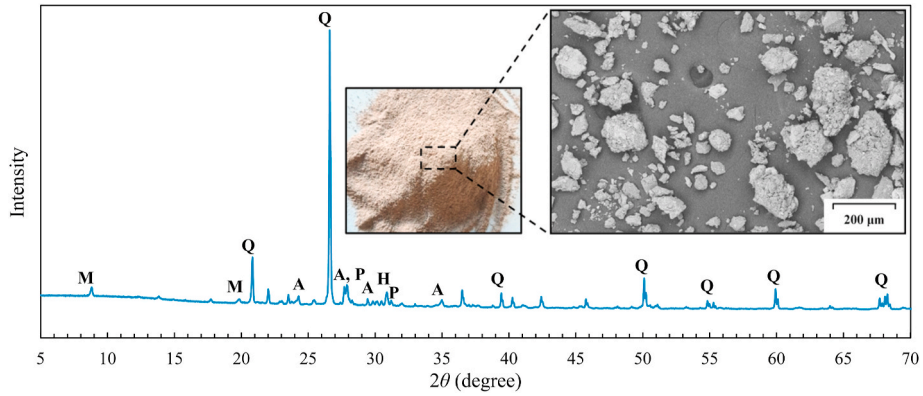

Fig. 1. XRD pattern and scanning electron micrograph of WAGT1; [M = muscovite ($KAl_3Si_3O_{10}(F,OH)_2$), A = albite ($NaAlSi_3O_8$), P = polyhalite ($Ca_2H_4K_2MgO_{18}S_4$), H = halite (NaCl), Q = quartz (SiO_2)].

Table 3
Mix proportions of UHPC mixes.

Mix ID.	Constituents (kg/m^3)								*w/b*
	Cement	Fly ash	Silica fume	Sand	WAGT1	Water	HRWR[a]	Defoaming agent[a]	
T0	794	140	233	969	–	212	14.7	1.3	0.182
T20	794	140	233	775	194	212	14.7	1.3	0.182
T40	794	140	233	581	388	212	14.7	1.3	0.182
T60	794	140	233	388	581	212	14.7	1.3	0.182
T80	794	140	233	194	775	212	14.7	1.3	0.182
T100	794	140	233	–	969	212	14.7	1.3	0.182

w/b = water to binder ratio.
[a] Solid content.

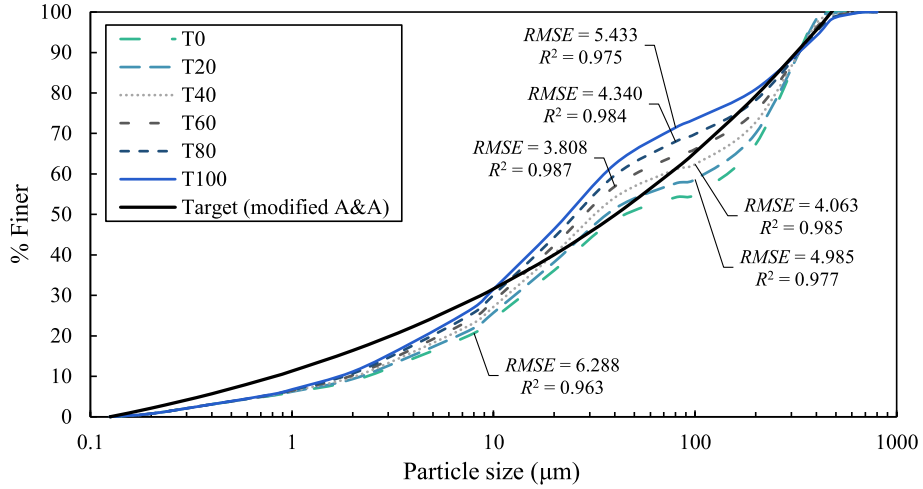

Fig. 3. Combined particle size distributions of UHPC mixes [*RMSE* = root-mean-square error, R^2 = determination coefficient].

packing density (ϕ) can be expressed by Eq. (2).

$$\phi = \frac{V_s}{V} \tag{2}$$

V is the volume of mould (mm^3), and V_s is the total volume of solid constituents (mm^3). V_s can be determined using Eq. (3).

$$V_s = \frac{M}{\rho_w}\left(\frac{\sum_{k=1}^{n}\frac{m_k}{G_k}}{m_w + \sum_{k=1}^{n} m_k}\right) \tag{3}$$

M is the mass of fresh UHPC occupying a volume of V after being subjected to 1 min of vibration (g), ρ_w is the density of water (g/mm^3), m_w is the mass of water per unit volume (g), m_k is the mass of each solid material per unit volume (g), G_k is the specific gravity of each dry material.

2.5. Mechanical tests

A compression testing machine with a capacity of 600 kN was used to perform the mechanical tests. The compressive strength tests were conducted at 7, 28, and 56 days according to guidelines of ASTM C109/C109M-16a (2016). Strain gauges were attached to the 28-day specimens for measuring their strains under compression. The elastic moduli of the specimens were calculated according to AS 1012.17 (1997). The splitting tensile strength tests were conducted at 28 days according to the guidelines of AS 1012.10 (2000). For each mechanical property, three specimens from each mix were tested.

2.6. Durability tests

The initial rate of absorption (IRA) tests were conducted using 100 × 100 mm plain cubes in accordance with the guidelines of IS 3495 (1992), and the water absorption (WA) tests were conducted using the same specimens as per the guidelines of AS/NZS 4456.17 (2003). To calculate the WA of each specimen **Eq. (4)** was used, and **Eq. (5)** was used to calculate the IRA. Three specimens from each mix were tested for both WA and IRA.

$$WA = \frac{100\left(m_i - m_f\right)}{m_i}\ (\%) \tag{4}$$

$$IRA = \frac{1000\left(m_{f,60} - m_i\right)}{A}\ \left(\mathrm{kg/m^2/min}\right) \tag{5}$$

m_i is the mass of oven-dried specimen (g), m_f is the mass of specimen after 24 h of immersion in water (g), $m_{f,60}$ is the mass of specimen after immersion of bottom 3 mm in water for 60 s (g), A is the bottom surface area of specimen (mm^2). Excess water on the specimen surface was wiped off using a damp cloth prior to measuring m_f or $m_{f,60}$.

Carbonation tests were carried out according to EN 13295 (2004) using 100 × 100 × 100 mm specimens. Each specimen was split into two halves. Phenolphthalein indicator (mixture of 1 g phenolphthalein powder, 70 ml ethanol, and 30 ml water) was then sprayed over the split section of each half. The colour change of each of the sections was observed to assess the carbonation resistance of the respective mix.

2.7. Leaching toxicity test

Leaching toxicity test was conducted for each UHPC mix using a slightly modified version of the approach mentioned in HJ 557 (2010). HJ 557 (2010) specifies the use of deionized water as leaching liquid. However, in this study, acetic acid (CH_3COOH) solution having a pH of 2.65 was chosen as the leaching liquid, complying with (Wang et al.,

2018). 100 g of crushed UHPC pieces with a maximum size of 3 mm were mixed with 1 L of leaching liquid. The mixture was subjected to 8 h of horizontal agitation and then left at a steady position for 16 h. After that, the supernatant was filtered through vacuum-filtration process (Fig. 4). The concentrations of heavy metals in the supernatant were measured using ICP-OES.

2.8. SEM analysis

SEM analysis was conducted using small pieces of T0 and T100. Backscattered scanning electron micrographs were captured using a field emission scanning electron microscope (FESEM).

3. Results and discussion

3.1. Fresh behaviour

The slump flow diameters of the fresh UHPC mixes are presented in Table 4. The slump flow diameters of the UHPC mixes decreased with the increasing replacement of sand by WAGT1. The reduction of the slump flow due to the incorporation of WAGT1 can be attributed to the non-uniform surface texture (Fig. 1) and fine size of WAGT1 particles (from Table 2, the median diameter of the sand was 237.3 μm, and the median diameter of WAGT1 was 141.4 μm). WAGT1, owing to their higher fineness, had higher surface-area per unit volume than that of the sand. Consequently, the inclusion of WAGT1, substituting certain percentage of the sand, increased the water demand to lubricate the particles present in fresh UHPC and reduced its slump flow (Shettima et al., 2016). Table 4 also presents the wet packing densities of the UHPC mixes. Although the UHPCs with WAGT1 exhibited lower slump than that of T0, their packing densities were, in general, higher than that of T0. This observation is in agreement with the *RMSE* and R^2 values presented in Fig. 3.

3.2. Compressive strength and splitting tensile strength

The 7-day, 28-day, and 56-day compressive strengths of the UHPCs with different replacements of quartz sand by WAGT1 are presented in Fig. 5(a). Up to 80% substitution of quartz sand by WAGT1, the 28-day compressive strength of UHPC remained either comparable to or slightly higher than that of T0. Similar phenomena were observed at 7 and 56 days. Substitution of sand by WAGT1, beyond 80%, impaired the strength of UHPC if compared with the strength of T0. The 28-day compressive strength of T0 was 142.6 MPa, and the 56-day strength was 151.9 MPa. The 28-day compressive strength changed by +4.6% for T20, −1.6% for T40 + 4.4% for T60, −1.3% for T80, and −7.6% for T100, with respect to the 28-day strength of T0. At 56 days, the compressive strength changed by +4.8% for T20, −0.1% for T40, +2.2% for T60, −2.0% for T80, and −6.6% for T100, with respect to that of T0. The compressive strength of UHPC incorporating WAGT1 can be influenced by different factors. High fineness of WAGT1 particles is likely to result in better particle packing, consequently higher packing density as can be seen from Table 4, and reduce porosity of hardened UHPC (Zhang et al., 2020a). Such feature of WAGT1 is expected to benefit the strength of UHPC. On the other hand, low crystalline quartz content (Table 2) and presence of softer minerals (e.g., muscovite, halite, polyhalite, etc.) in WAGT1 (Fig. 1) tend to impart low elastic modulus to UHPC (Perkins, 1999). Low quartz content of WAGT1, as a result, is likely to cause reduced strength compared to UHPC with quartz sand (Zhao et al., 2014). Improved packing density of UHPC attained through WAGT1 incorporation most likely helped the UHPCs with up to 80% WAGT1 achieve strength comparable to or slightly higher than that of T0. The reduction in strength of T100 can be attributed to the low quartz content in WAGT1. The 28-day compressive strengths of the UHPCs made with up to 100% substitution of quartz sand by WAGT1 were greater than 120 MPa. T100 was observed to achieve 28-day strength (131.8 MPa) comparable to that presented in (Pyo et al., 2018) for UHPC with 30% quartz based tailings as aggregate, and higher than that presented in (Zhao et al., 2014) for UHPC with 100% iron ore tailings (Table 1). UHPCs made with up to 60% substitution of quartz sand by WAGT1 attained compressive strengths greater than 150 MPa at 56 days, without employing any special curing (e.g., autoclaving, heat-curing, steam-curing, etc.). It is also worth noting that the ECO-UHPCs developed in this study exhibited substantially higher compressive strengths than conventional NSC (exhibiting strength usually less than 40 MPa). The ECO-UHPC mixes can be used to construct slenderer structural members (Fehling et al., 2015), and thinner roads or pavements (Larrard and Sedran, 2011).

Table 4
Fresh properties of UHPC mixes.

Mix	T0	T20	T40	T60	T80	T100
Slum flow diameter (mm)	210	170	166.5	155	145	105
Wet packing density	0.771	0.793	0.795	0.808	0.789	0.792

The 28-day splitting tensile strengths of the UHPCs are presented in Fig. 5(b). The splitting tensile strength of T0 was 7.51 MPa. The splitting tensile strength changed by +8.9% for T20, +13.2% for T40, +5.5% for T60, −9.2% for T80, and −2.8% for T100, with respect to that of T0. Dense particle packing facilitated by high fineness of WAGT1 positively influenced the splitting tensile strengths of the UHPCs with up to 60% WAGT1. However, presence of soft minerals on the surfaces of WAGT1 particles perhaps resulted in weak bonds between the concrete matrix and WAGT1 particles (Alsalman et al., 2017). Formation of such weak WAGT1 particle – matrix bonds was possibly the governing factor to impart reduced splitting tensile strengths to the UHPCs with WAGT1

(a) **(b)**

Fig. 4. Leachate sample preparation for leaching toxicity test – **(a)** horizontal shaking of UHPC pieces and leaching liquid, and **(b)** vacuum filtration of leachate.

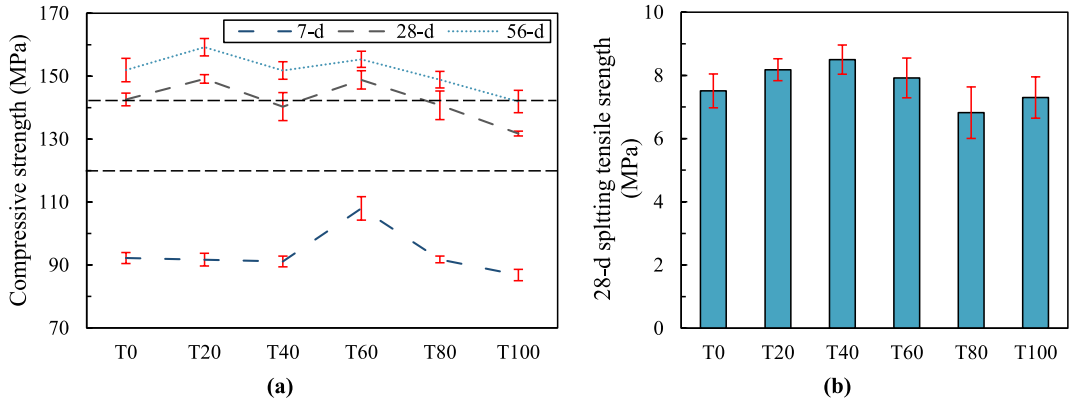

Fig. 5. (a) Compressive strength results, and **(b)** 28-day splitting tensile strength results of UHPCs.

content of more than 60%.

3.3. Elastic modulus

The 28-day elastic moduli of the UHPC mixes are presented in Fig. 6 (a). The results show that the elastic modulus of UHPC generally decreased with the increase of WAGT1 content. This is most likely because WAGT1 were softer than the quartz sand owing to the lower quartz content (Table 2) and presence of softer minerals (e.g., muscovite, halite, polyhalite, etc.) in WAGT1 (Fig. 1). The 28-day elastic modulus of T0 was 42.6 GPa. The elastic modulus decreased by 1.4% for T20, 4.9% for T40, 5.8% for T60, 7.2% for T80, and 10.9% for T100, with respect to the elastic modulus of T0.

The elastic moduli of the UHPC mixes are plotted against the square roots of their respective compressive strengths [$\sqrt{(f_c)}$] in Fig. 6(b). The R^2 obtained for the line of best fit was found to be 0.47, and the *RMSE* was found to be 1.12. In Fig. 6(c), the elastic moduli of the UHPC mixes are plotted against their respective $\sqrt{(f_c)}$ to ϕ (wet packing density) ratios. Fig. 6(c) shows a low scatter of the presented data compared to that of the data presented in Fig. 6(b). The R^2 between the line of best fit and the data presented in Fig. 6(c) was found to be 0.90, and the *RMSE* was found to be 0.50. Lower scatter of the data in Fig. 6(c) implies that the elastic modulus of UHPC incorporating WAGT1 can be better represented as a function of $\sqrt{(f_c)}/\phi$ than as a function of $\sqrt{(f_c)}$. This is possibly because, in comparison to the compressive strength, the elastic modulus of UHPC incorporating WAGT1 is less sensitive to the variation of the packing density. Due to limited datapoints, the present study did not propose any equation. The study can be extended in future

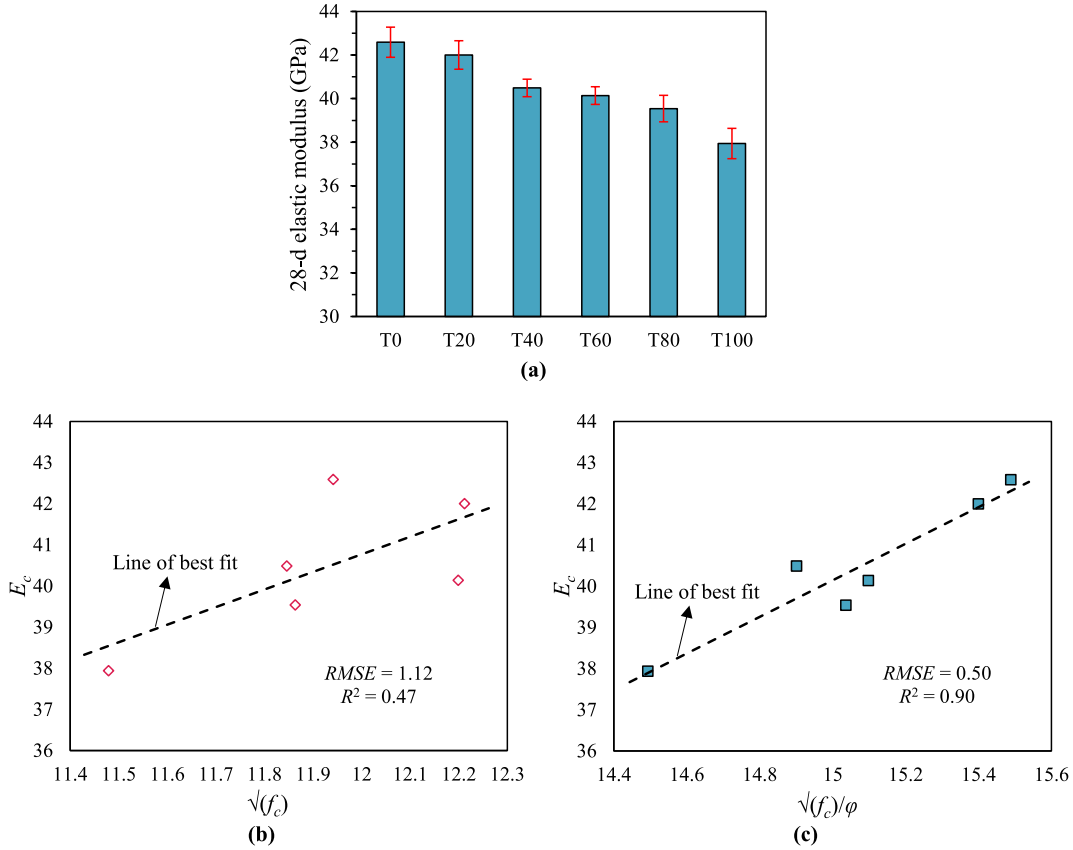

Fig. 6. (a) 28-day elastic moduli of UHPCs, **(b)** E_c as a function of $\sqrt{(f_c)}$, and **(c)** E_c as a function of $\sqrt{(f_c)}/\phi$; [E_c = elastic modulus, f_c = compressive strength, ϕ = wet packing density].

compiling more elastic modulus, compressive strength, and wet packing density results in order to develop a relationship for estimating the elastic modulus of UHPC incorporating WAGT1.

3.4. Durability

Fig. 7 shows the water absorption (WA) and the initial rate of absorption (IRA) test results of the UHPCs at 28 days. The WAs and IRAs of the UHPCs incorporating WAGT1 were generally lower than those of T0. Zhang et al. (2020a) observed similar behaviour in their investigation when manufactured sand was replaced by finer iron ore tailings. Fine particles of WAGT1 most likely helped fill the micro-voids of UHPC mix, and helped UHPC to attain lower 28-day WA and IRA (Gupta and Vyas, 2018). The 28-day WA was 1.123% for T0, 1.121% for T20, 1.028% for T40, 1.012% for T60, 1.011% for T80, and 0.866% for T100. The IRA was 0.082 kg/m^2/min for T0, 0.067 kg/m^2/min for T20, 0.078 kg/m^2/min for T40, 0.055 kg/m^2/min for T60, 0.046 kg/m^2/min for T80, and 0.055 kg/m^2/min for T100, at 28 days. It was interesting to observe that the WAs of all the UHPCs were less than 1.5%. Concrete exhibiting WA less than 2% is considered durable, for construction works with fifty-year design life in coastal regions (Ahmed et al., 2021). The WA of NSC is typically much higher than 3.5% (Neville, 2011). The ECO-UHPCs developed in this study can be used to prepare more durable structures, pavements, or roads than those built with NSC.

Fig. 8 shows the colour changes of the cut sections of elevated CO_2 cured UHPC specimens upon the application of phenolphthalein solution. Dark pink colour was observed throughout the cross-sections of all the UHPC specimens. This implies no visible carbonation front was present in any of the specimens. In other words, the depth of carbonation was below the detection limit (<0.5 mm) for all the UHPCs. These observations on the UHPCs incorporating different contents of WAGT1 agree with the results obtained by Scheydt and Müller (2012) for conventional UHPC. Promising carbonation resistances of the UHPCs, irrespective of their aggregate types, can mainly be attributed to their very dense matrices owing to the use of very low *w/b* ratio (= 0.182) and the use of silica fume. The dense microstructures of the UHPCs substantially restricted the diffusion of CO_2 into the concretes and resulted in almost zero carbonation depths.

3.5. Leaching toxicity

The concentrations of the heavy metals in the leachates extracted from different UHPC – leaching liquid mixtures are presented in Table 5. For all the UHPCs, the concentrations of the heavy metals were well below their respective regulatory thresholds set by different environment protection guidelines and regulations. Such low concentrations of the toxic metals in the leachates, compared to their respective regulatory thresholds, indicate safe use of WAGT1 in UHPC. Long-term leaching test can be conducted in future for gaining deeper insight into the leaching behaviour of heavy metals in UHPCs incorporating WAGT1.

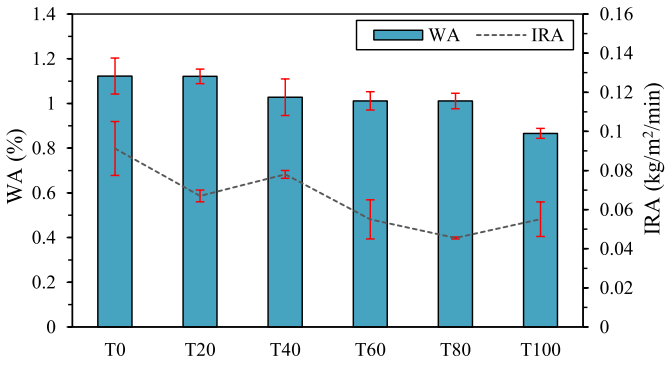

Fig. 7. Water absorption and initial rate of absorption results of UHPCs.

Three factors possibly influenced the leaching toxicity test results of the current study. First, concentrations of some of the heavy metals (e.g., Cd, Pb) were very low in the as-received WAGT1. Second, certain heavy metals in WAGT1 were perhaps present in oxidation states which show low leachability or low mobility (e.g., possible presence of arsenic as arsenate) (Shrivastava et al., 2015). Third, the very dense microstructure of UHPC highly restricted the leaching behaviour of toxic metals present in WAGT1 (Wang et al., 2018). The leaching behaviour of leachable heavy metals from a particular type of tailings in UHPC, compared to their behaviours in low-strength and normal-strength mortars, can be illustrated by the schematic diagram shown in Fig. 9. In comparison to low-strength and normal-strength mortars, UHPC is very dense and less porous because of its low *w/b* ratio and the presence of silica fume in it. The binder to aggregate ratio of UHPC is also much higher than those of low-strength and normal-strength mortars. Because of this, the aggregate particles in UHPC are covered with thick layers of paste. Foregoing features of UHPC have the potential to provide substantial hindrance to the leaching of heavy metals from the tailings present in it (Liu et al., 2020b).

3.6. Microstructure analysis

Fig. 10(a) shows the backscattered electron micrograph of T0, and Fig. 10(b) shows that of T100. Because of the low *w/b* ratio, a lot of cement particles (white features in the matrix) were seen to remain unreacted in both T0 and T100 samples. Larger pores were observed in the matrix of T0. This indicates denser packing was achieved for T100 than that of T0. The observation is consistent with the higher wet packing density of T100 than that of T0 (Table 4). The WAGT1 particles exhibited bright colour in the backscattered electron microscopy, compared to the sand particles. This is because the sand mainly contained Si-based quartz whereas WAGT1, apart from Si-based quartz, had minerals incorporating heavier elements (such as, Ca, Fe, etc.) (Table 2). WAGT1 particles were generally observed to be surrounded by wider cracks than sand particles. This may be attributed to the weak bonding between WAGT1 particles and matrix, occurring because of the presence of soft minerals in WAGT1 (Alsalman et al., 2017). Such property of WAGT1 imparted low strength to T100 if compared with the strength of T0 (Perkins, 1999).

3.7. Economic and environmental evaluation

Fig. 11(a) presents the estimated material costs and combined material and transportation costs of UHPCs with different WAGT1. The estimated CO_2 footprints of the UHPC mixes, based on both the CO_2 emission from materials and the combined emission from materials and transportation, are presented in Fig. 11(b).

Table 6 presents the data used for the calculation of the material costs and CO_2 footprints of different UHPC mixes. The material costs and CO_2 footprints of the cement, silica fume, fly ash, and quartz sand reported in (Ahmed et al., 2021) were used for the calculation of the material cost and CO_2 footprint of T0. For calculating the material costs and CO_2 footprints of the mixes with WAGT1, approximate cost (A $53/t) and CO_2 emission (2.1 kg/t) for screening out coarse rock fraction from raw WAGT1 were considered, in addition to the costs and CO_2 footprints of other materials reported in (Ahmed et al., 2021). In order to determine the costs and CO_2 emissions from transportation, the cement, silica fume, fly ash, quartz sand, and chemical admixtures (HRWR and defoamer) were assumed to be transported from local sources in WA. The cement source was assumed to be located at a distance of 20.1 km from the Perth CBD (central business district), silica fume source at a distance of 152 km, fly ash source at a distance of 209 km, quartz sand source at a distance of 28.9 km, and the source of chemical admixtures at a distance of 23 km. Due to the confidentiality agreement the exact distance of Mine 1 from the CBD is not mentioned here. The cost of transport (articulated truck freight) was considered to be A$0.09/t/km

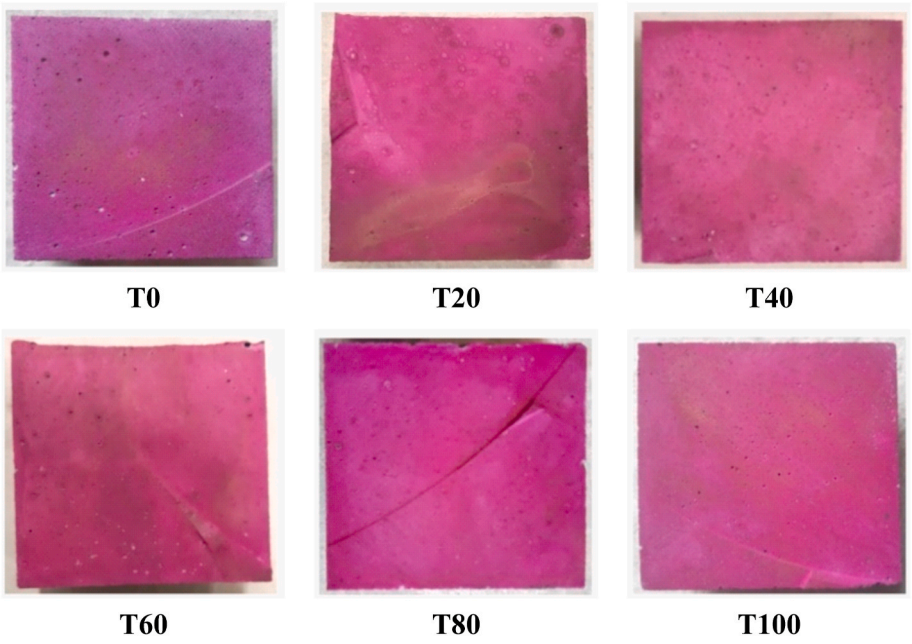

Fig. 8. Illustration of carbonation resistances of UHPCs.

Table 5
Concentrations (mg/L) of heavy metals in leachate samples.

Heavy metal	Sample						Regulatory threshold			
	T0	T20	T40	T60	T80	T100	NSW EPA (2014)	GB 5085.3 (2007)	GB 16889 (2008)	40 CFR 261.24
Zn	0.181	0.192	0.215	0.159	0.149	0.162	–	100	100	–
Cd	<0.001	<0.001	<0.001	<0.001	<0.001	<0.001	1	1	0.15	1
As	<0.005	<0.005	<0.005	<0.005	0.006	<0.005	5	5	0.3	5
Pb	<0.005	<0.005	<0.005	<0.005	<0.005	<0.005	5	5	0.25	5
Cu	0.029	0.046	0.067	0.070	0.076	0.139	–	100	40	–

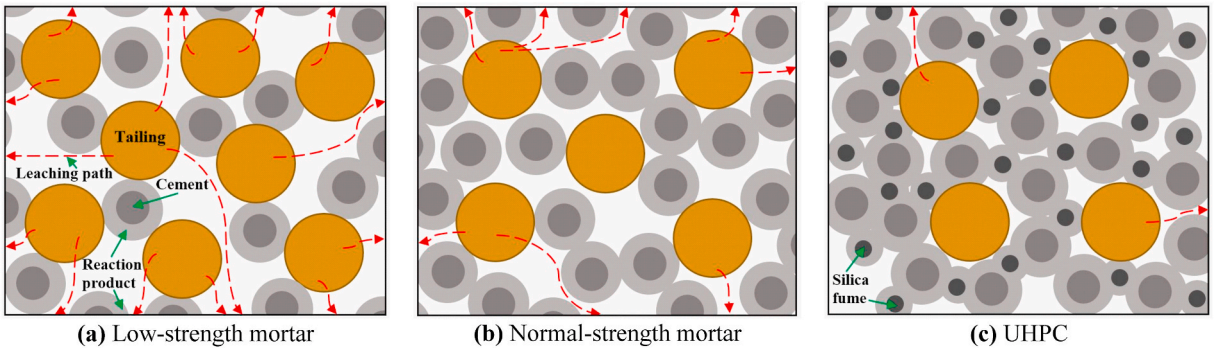

Fig. 9. Leaching behaviour of leachable heavy metals from tailings in – **(a)** low-strength mortar, **(b)** normal-strength mortar, and **(c)** UHPC.

(Shaikh et al., 2019), and CO_2 emission was considered to be 0.071 kg/t/km (O'Brien et al., 2009).

The estimated material cost of T0 is A$1586/m^3. The material cost can be reduced by 6.2% for T20, 12.4% for T40, 18.6% for T60, 24.8% for T80, and 31% for T100, with respect to the cost of T0. Very low processing cost of WAGT1, in comparison to the cost related to the energy-intensive processes of extraction, grinding, and refining of quartz sand, imparts reduced material costs to the mixes with WAGT1. The combined material and transportation costs of UHPC, for constructions near both Perth CBD and Mine 1, also reduce when quartz sand is replaced by WAGT1. The combined material and transportation cost reduces by 4.3% for T20, 8.6% for T40, 12.9% for T60, 17.2% for T80, and 21.6% for T100, with respect to the cost of T0, for construction near the CBD. For construction in the area near Mine 1, the combined cost can be reduced by 6.6% for T20, 13.2% for T40, 19.9% for T60, 26.5% for T80, and 33.1% for T100.

The material CO_2 footprint of UHPC reduces slightly when quartz sand is substituted by WAGT1. This can mainly be attributed to the reduction/omission of the extraction, grinding, and refining phases of quartz sand manufacturing process when WAGT1 are used. However, the reduction in material CO_2 footprint of UHPC, for certain replacement of sand by WAGT1, is less pronounced compared to the reduction in material cost. This is because the use of high-volume cement for UHPC production is the major contributor (90%–92%) to the material CO_2 footprint of UHPC. For construction near the CBD, the combined CO_2 emission from materials and transportation increases by up to 11.6%

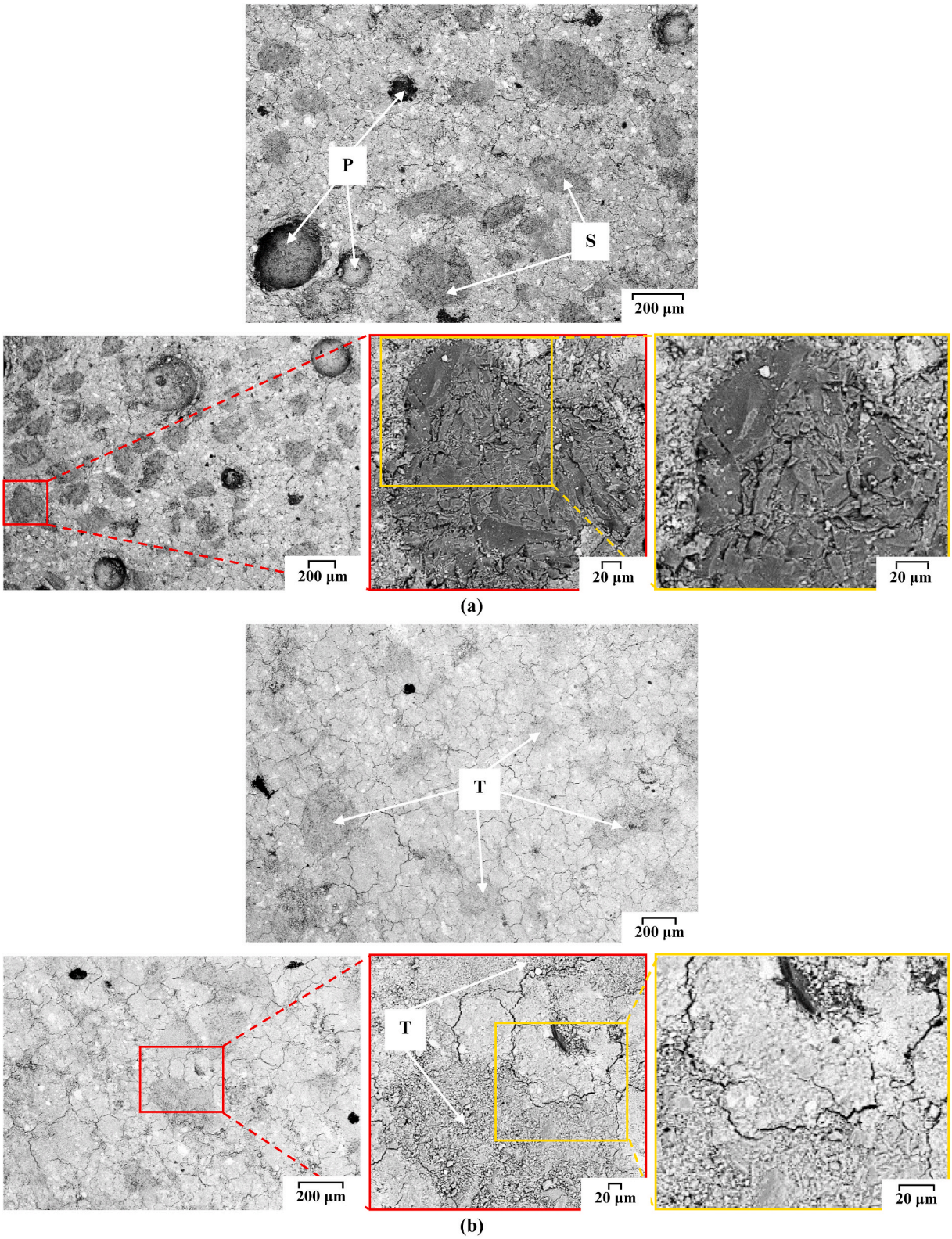

Fig. 10. Backscattered electron micrographs of **(a)** T0, and **(b)** T100; [P = pore, S = quartz sand, T = WAGT1].

when quartz sand is replaced by WAGT1. This can be attributed to the large distance of Mine 1 from the CBD, compared to the distance between the quartz sand source and the CBD. Studies can be carried out in future investigating the influences of using gold tailings from mines nearer to the CBD on the properties of UHPC. However, for construction near Mine 1, the combined CO_2 emission from materials and transportation can be decreased by up 12.1% if WAGT1 are used instead of quartz sand.

Along with the CO_2 emission, extraction and grinding processes of quartz sand have a number of other environmental consequences. Some of the most important ones, as indicated in (Gavriletea, 2017), are – deforestation, loss of biodiversity, soil degradation, lowering of water

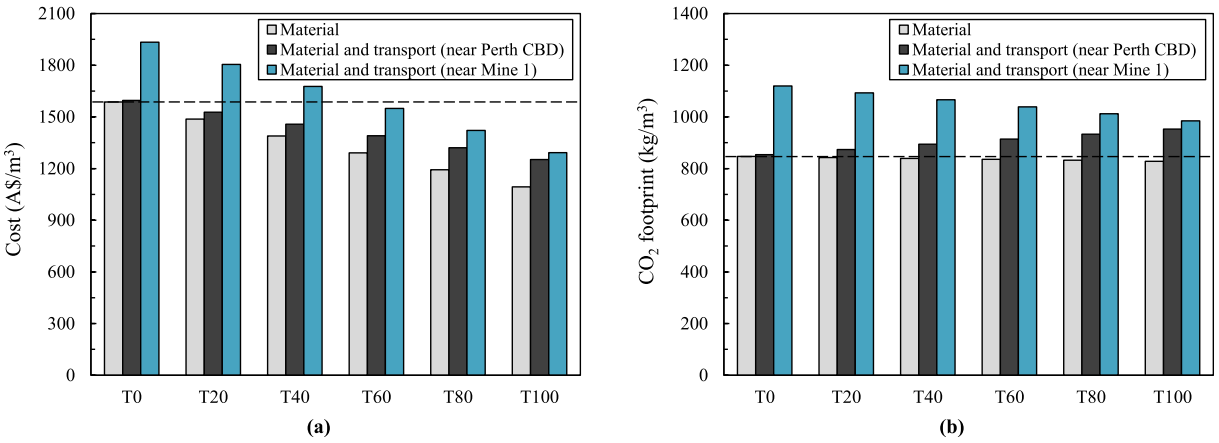

Fig. 11. (a) Costs, and **(b)** CO_2 footprints of UHPC mixes.

Table 6
CO_2 footprints and costs of materials.

Material	Cement	Silica fume	Fly ash	Quartz sand	WAGT1	Water	Admixture[a]
Material CO_2 footprint (kg/t)	959[b]	82[b]	93[b]	21[b]	2.1	1[b]	508[b]
Material cost (A$/kg)	0.75[b]	0.52[b]	0.51[b]	0.56[b]	0.053	0.0015[b]	4.4[b] (HRWR) 3.23[b] (defoaming agent)

[a] Including liquid content.
[b] Adopted from (Ahmed et al., 2021).

table, particulate matter air pollution during grinding, etc. The natural sources of quartz sand are depleting so drastically that the demand for sand may surpass the supply by mid-century (Bendixen et al., 2019). Long-term continuous disposal of tailings is also associated with several concerns. Fine fraction of the disposed tailings can pollute the surrounding air (Dong et al., 2019). To facilitate long-term disposal, construction of new tailings storage facilities (TSFs) or gradual enlargement of the existing tailings dam structure is often required. Construction of new TSFs requires the use of additional landmasses. Again, gradual enlargement of the tailings dam structure increases the risk of dam failure as well as the difficulty of tailings management (Edraki et al., 2014). Dam failure may pose a severe threat to the safety of the workers and the people residing in the locality, and can even lead to the pollution of surrounding surface and ground waters, soil, crops, etc. (Ince, 2019). Although WAGT1 at Mine 1 are currently managed as per the guidelines of ANCOLD (Australian National Committee on Large Dams) and ICMM (International Council on Mining and Metals), continuous disposal of WAGT1 may make the management more challenging in future years. The problems, related both to the manufacturing process of fine quartz sand and to the disposal of WAGT1, can be addressed to some extent if quartz sand in UHPC is partially or fully substituted by WAGT1.

4. Conclusion

Based on the results and discussion presented in the preceding section, the following conclusions can be drawn:

1. UHPCs, incorporating up to 80% WAGT1, exhibit compressive strength comparable to or slightly higher than the compressive strength of UHPC with 100% quartz sand. The 28-day compressive strength of UHPC with 20%–80% WAGT1 changes by −1.3% to +4.58%, with respect to the 28-day strength of UHPC with 100% quartz sand. UHPC with 100% WAGT1 exhibits 7.6% lower compressive strength with respect to that of UHPC with 100% quartz sand. However, strength greater than 120 MPa is achievable at 28 days for UHPC with 100% WAGT1. 28-day strength achieved in this study for UHPC incorporating 100% WAGT1 (131.8 MPa) is also comparable to or higher than those presented in the previous studies for ambient temperature cured UHPCs with quartz based tailings and iron ore tailings. UHPCs made with up to 60% substitution of quartz sand by WAGT1 can attain compressive strengths greater than 150 MPa at 56 days without employing any special curing.
2. UHPCs with up to 60% WAGT1 generally exhibit higher (5.5%–13.2%) splitting tensile strengths than that of UHPC without WAGT1. Beyond 60% replacement, splitting tensile strength generally decreases (2.8%–9.2%). The elastic modulus of UHPC generally reduces (up to 10.9%) as quartz sand is replaced by WAGT1.
3. The flowability of fresh UHPC reduces with the substitution of quartz sand by WAGT1. However, better wet packing density can be attained for UHPC with WAGT1 than that of UHPC with 100% quartz sand.
4. UHPCs incorporating WAGT1 generally exhibit lower water absorptions and initial rate of absorptions than those of UHPC with 100% quartz sand. UHPC, irrespective of WAGT1 content, shows substantial resistance to carbonation.
5. The leachability of toxic metals from UHPC, irrespective of its WAGT1 content, lies well below the regulatory thresholds. Long-term leaching test can be conducted in future for gaining further insight into the leaching behaviour of heavy metals in UHPCs incorporating WAGT1.
6. The combined material and transportation cost of UHPC can be reduced by up to 33.1%, for construction in the area near Mine 1. For construction near the Perth CBD, the combined cost reduces by up to 21.6% when quartz sand is replaced by WAGT1.
7. For construction near Mine 1, the combined CO_2 emission from materials and transport can be reduced by up to 12.1% when quartz sand is replaced by WAGT1. However, the combined CO_2 emission can increase by up to 11.6%, for construction near the Perth CBD. Studies can be carried out in future to investigate the properties of UHPCs incorporating gold tailings from mines nearer to the CBD, which may be economically and environmentally more attractive for construction near the CBD.
8. Utilization of WAGT1 as quartz sand substitute for UHPC production, especially near Mine 1, can reduce the demand for quartz sand to

some extent. In the long run, negative environmental impacts of quartz sand extraction can be reduced (e.g., deforestation, loss of biodiversity, soil degradation, lowering of water table, etc.). Cleaner UHPC production in such a way can also help prevent concerns/problems, related to the long-term disposal of WAGT1, from arising in the future (e.g., need for new landmasses, risk of tailings dam failure, etc.).

In summary, UHPC exhibiting 28-day compressive strength greater than 120 MPa, water tightness better than UHPC incorporating quartz sand, and carbonation resistance similar to conventional UHPC can be produced using WAGT1 as aggregate. The cost and CO_2 emission can also be reduced for construction near Mine 1 if WAGT1 is used instead of quartz sand. The results imply, in the area near Mine 1, the use of WAGT1 can economically and environmentally, as well as in terms of durability, be a better option than quartz sand for construction works that require UHPC with 28-strength in excess of 120 MPa. Moreover, the ECO-UHPCs developed in this study, owing to their substantially higher strength and better durability than NSC, can be used to construct slenderer and/or more durable structural members, pavements, or roads than those built with NSC.

Declaration of competing interest

The authors declare that they have no known competing financial interests or personal relationships that could have appeared to influence the work reported in this paper.

Acknowledgements

The authors acknowledge the facilities provided by the Centre for Microscopy, Characterization & Analysis, The University of Western Australia for performing the XRD and SEM analyses. Special thanks are given to Mr. Andrew van de Ven for his support to conduct the leaching toxicity test. The research was carried out while the first author was a recipient of a University Postgraduate Award and the Australian Government Research Training Program Scholarship at The University of Western Australia.

Appendix A. Supplementary data

Supplementary data to this article can be found online at https://doi.org/10.1016/j.clet.2021.100176.

References

40 CFR 261.24, 40 CFR 261.24, Toxicity Characteristic.
Ahmed, T., Elchalakani, M., Karrech, A., Dong, M., Ali, M.S.M., Yang, H., 2021. ECO-UHPC with high-volume Class-F fly ash: new insight into mechanical and durability properties. J. Mater. Civ. Eng. 33, 0003726 https://doi.org/10.1061/(ASCE)MT.1943-5533.0003726.
Alsalman, A., Dang, C.N., Prinz, G.S., Hale, W.M., 2017. Evaluation of modulus of elasticity of ultra-high performance concrete. Construct. Build. Mater. 153, 918–928. https://doi.org/10.1016/j.conbuildmat.2017.07.158.
AS 1012.10, 2000. Methods of Testing Concrete: Determination of Indirect Tensile Strength of Concrete Cylinders ("Brazil" or Splitting Test. In:).
AS 1012.17, 1997. Methods of Testing Concrete: Determination of the Static Chord Modulus of Elasticity and Poisson's Ratio of Concrete Specimens.
AS 1012.3.5, 2015. Methods of Testing Concrete: Determination of Properties Related to the Consistency of Concrete - Slump Flow, T500 and J-Ring Test.
AS/NZS 3582.3, 2016. Supplementary Cementitious Materials for Use with Portland and Blended Cement - Amorphous Silica.
AS/NZS 4456.17, 2003. Masonry Units and Segmental Pavers and Flags - Methods of Test: Determining Initial Rate of Absorption (Suction).
ASTM C150/C150M-16, 2016. Standard Specification for Portland Cement. West Conshohocken, PA.
ASTM C618-19, 2019. Standard Specification for Coal Fly Ash and Raw or Calcined Natural Pozzolan for Use in Concrete. https://doi.org/10.1520/C0618-19. West Conshohocken, PA.
ASTMC109 /C109M-16a, 2016. Standard Test Method for Compressive Strength of Hydraulic Cement Mortars (Using 2-in. Or [50-mm] Cube Specimens). https://doi.org/10.1520/C0109_C0109M-16A. West Conshohocken, PA.
Bendixen, M., Best, J., Hackney, C., Iversen, L.L., 2019. Time is running out for sand. Nature 571, 29–31. https://doi.org/10.1038/d41586-019-02042-4.
Courtial, M., De Noirfontaine, M.N., Dunstetter, F., Signes-Frehel, M., Mounanga, P., Cherkaoui, K., Khelidj, A., 2013. Effect of polycarboxylate and crushed quartz in UHPC: microstructural investigation. Construct. Build. Mater. 44, 699–705. https://doi.org/10.1016/j.conbuildmat.2013.03.077.
Dong, L., Tong, X., Li, X., Zhou, J., Wang, S., Liu, B., 2019. Some developments and new insights of environmental problems and deep mining strategy for cleaner production in mines. J. Clean. Prod. 210, 1562–1578. https://doi.org/10.1016/j.jclepro.2018.10.291.
Edraki, M., Baumgartl, T., Manlapig, E., Bradshaw, D., Franks, D.M., Moran, C.J., 2014. Designing mine tailings for better environmental, social and economic outcomes: a review of alternative approaches. J. Clean. Prod. 84, 411–420. https://doi.org/10.1016/j.jclepro.2014.04.079.
EN 13295, 2004. Products and Systems for the Protection and Repair of Concrete Structures - Test Methods - Determination of Resistance to Carbonation.
Fehling, E., Schmidt, M., Walraven, J., Leutbecher, T., Fröhlich, S., 2015. Ultra-high performance concrete UHPC: fundamentals, design, examples, ultra-high performance concrete UHPC: fundamentals, design, examples. https://doi.org/10.1002/9783433604076.
Fisonga, M., Wang, F., Mutambo, V., 2019. Sustainable utilization of copper tailings and tyre-derived aggregates in highway concrete traffic barriers. Construct. Build. Mater. 216, 29–39. https://doi.org/10.1016/j.conbuildmat.2019.05.008.
Gao, S., Cui, X., Kang, S., Ding, Y., 2020. Sustainable applications for utilizing molybdenum tailings in concrete. J. Clean. Prod. 266, 122020. https://doi.org/10.1016/j.jclepro.2020.122020.
Gavriletea, M.D., 2017. Environmental impacts of sand exploitation: analysis of sand market. Sustain 9, 1118. https://doi.org/10.3390/su9071118.
GB 16889, 2008. Standard for Pollution Control on the Landfill Site of Municipal Solid Waste.
GB 5085.3, 2007. Identification Standards for Hazardous Wastes - Identification for Extraction Toxicity.
Gupta, L.K., Vyas, A.K., 2018. Impact on mechanical properties of cement sand mortar containing waste granite powder. Construct. Build. Mater. 191, 155–164. https://doi.org/10.1016/j.conbuildmat.2018.09.203.
Gupta, R.C., Mehra, P., Thomas, B.S., 2017. Utilization of copper tailing in developing sustainable and durable concrete. J. Mater. Civ. Eng. 29, 04016274 https://doi.org/10.1061/(asce)mt.1943-5533.0001813.
HJ 557, 2010. Solid Waste—extraction Procedure for Leaching Toxicity — Horizontal Vibration Method.
Huang, H., Gao, X., Jia, D., 2019. Effects of rheological performance, antifoaming admixture, and mixing procedure on air bubbles and strength of UHPC. J. Mater. Civ. Eng. 31, 04019016 https://doi.org/10.1061/(asce)mt.1943-5533.0002651.
Ince, C., 2019. Reusing gold-mine tailings in cement mortars: mechanical properties and socio-economic developments for the Lefke-Xeros area of Cyprus. J. Clean. Prod. 238, 117871. https://doi.org/10.1016/j.jclepro.2019.117871.
IS 3495 (Part 2), 1992. Methods of Tests of Burnt Clay Building Bricks, Part 2: Determination of Water Absorption. New Delhi.
Jiao, Y., Zhang, Y., Guo, M., Zhang, L., Ning, H., Liu, S., 2020. Mechanical and fracture properties of ultra-high performance concrete (UHPC) containing waste glass sand as partial replacement material. J. Clean. Prod. 277, 123501. https://doi.org/10.1016/j.jclepro.2020.123501.
Kathirvel, P., Kwon, S.J., Lee, H.S., Karthick, S., Saraswathy, V., 2018. Graphite ore tailings as partial replacement of sand in concrete. ACI Mater. J. 115, 481–492. https://doi.org/10.14359/51702191.
Kim, H., Koh, T., Pyo, S., 2016. Enhancing flowability and sustainability of ultra high performance concrete incorporating high replacement levels of industrial slags. Construct. Build. Mater. 123, 153–160. https://doi.org/10.1016/j.conbuildmat.2016.06.134.
Kinnunen, P., Ismailov, A., Solismaa, S., Sreenivasan, H., Räisänen, M.L., Levänen, E., Illikainen, M., 2018. Recycling mine tailings in chemically bonded ceramics – a review. J. Clean. Prod. 174, 634–649. https://doi.org/10.1016/j.jclepro.2017.10.280.
Larrard, F. de, Sedran, T., 2011. High and ultra-High performance concrete in pavement: tools for the road eternity. In: 9th International Symposium on High Performance Concrete: Design, Verification and Utilization. Rotorua, New Zealand hal-00877025.
Li, T., Wang, S., Xu, F., Meng, X., Li, B., Zhan, M., 2020. Study of the basic mechanical properties and degradation mechanism of recycled concrete with tailings before and after carbonation. J. Clean. Prod. 259, 120923. https://doi.org/10.1016/j.jclepro.2020.120923.
Liu, H., Li, B., Xue, J., Hu, J., Zhang, J., 2020a. Mechanical and electroconductivity properties of graphite tailings concrete. Ann. Mater. Sci. Eng. 2020, 9385097. https://doi.org/10.1155/2020/9385097.
Liu, T., Wei, H., Zou, D., Zhou, A., Jian, H., 2020b. Utilization of waste cathode ray tube funnel glass for ultra-high performance concrete. J. Clean. Prod. 249, 119333. https://doi.org/10.1016/j.jclepro.2019.119333.
Logsdon, M.J., Hagelstein, K., Mudder, T.I., 1999. The Management of Cyanide in Gold Extraction. Ottawa.
Nematollahi, B., MR, R.S., Voo, Y.L., 2011. Ultra high performance concrete (UHPC) technology from material to structure : a review. In: Ghani, A.N.A., Mydin, M.A.O., Abas, N.F. (Eds.), International Building & Infrastructure Technology Conference. Universiti Sains Malaysia, Penang, Malaysia, pp. 359–366.
Neville, A.M., 2011. Properties of Concrete, fifth ed. Pearson, London, UK.
NSW EPA, 2014. Waste Classification Guidelines – Part 1: Classification of Waste. Sydney.

O'Brien, K.R., Ménaché, J., O'Moore, L.M., 2009. Impact of fly ash content and fly ash transportation distance on embodied greenhouse gas emissions and water consumption in concrete. Int. J. Life Cycle Assess. 14, 621–629. https://doi.org/10.1007/s11367-009-0105-5.

Perkins, W.G., 1999. Polymer toughness and impact resistance. Polym. Eng. Sci. 39, 2445–2460. https://doi.org/10.1002/pen.11632.

Protasio, F.N.M., Avillez, R.R. de, Letichevsky, S., Silva, F. de A., 2021. The use of iron ore tailings obtained from the Germano dam in the production of a sustainable concrete. J. Clean. Prod. 278, 123929. https://doi.org/10.1016/j.jclepro.2020.123929.

Pyo, S., Tafesse, M., Kim, B.J., Kim, H.K., 2018. Effects of quartz-based mine tailings on characteristics and leaching behavior of ultra-high performance concrete. Construct. Build. Mater. 166, 110–117. https://doi.org/10.1016/j.conbuildmat.2018.01.087.

Scheydt, J., Müller, H., 2012. Microstructure of ultra high performance concrete (UHPC) and its impact on durability. 3rd Int. Symp. Ultra High Perform. Concr. 349–356.

Shaikh, F.U.A., Nath, P., Hosan, A., John, M., Biswas, W.K., 2019. Sustainability assessment of recycled aggregates concrete mixes containing industrial by-products. Mater. Today Sustain. 5 https://doi.org/10.1016/j.mtsust.2019.100013.

Shettima, A.U., Hussin, M.W., Ahmad, Y., Mirza, J., 2016. Evaluation of iron ore tailings as replacement for fine aggregate in concrete. Construct. Build. Mater. 120, 72–79. https://doi.org/10.1016/j.conbuildmat.2016.05.095.

Shrivastava, A., Ghosh, D., Dash, A., Bose, S., 2015. Arsenic contamination in soil and sediment in India: sources, effects, and remediation. Curr. Pollut. Reports 1, 35–46. https://doi.org/10.1007/s40726-015-0004-2.

Thomas, B.S., Damare, A., Gupta, R.C., 2013. Strength and durability characteristics of copper tailing concrete. Construct. Build. Mater. 48, 894–900. https://doi.org/10.1016/j.conbuildmat.2013.07.075.

Tian, Z.X., Zhao, Z.H., Dai, C.Q., Liu, S.J., 2016. Experimental study on the properties of concrete mixed with iron ore tailings. Adv. Mater. Sci. Eng. 2016 8606505. https://doi.org/10.1155/2016/8606505.

UNEP, 2014. Sand, Rarer than One Thinks.

Wang, X., Yu, R., Shui, Z., Zhao, Z., Song, Q., Yang, B., Fan, D., 2018. Development of a novel cleaner construction product: ultra-high performance concrete incorporating lead-zinc tailings. J. Clean. Prod. 196, 172–182. https://doi.org/10.1016/j.jclepro.2018.06.058.

Wong, H.H.C., Kwan, A.K.H., 2008. Packing density of cementitious materials: Part 1-measurement using a wet packing method. Mater. Struct. Constr. 41, 689–701. https://doi.org/10.1617/s11527-007-9274-5.

Xu, W., Wen, X., Wei, J., Xu, P., Zhang, B., Yu, Q., Ma, H., 2018. Feasibility of kaolin tailing sand to be as an environmentally friendly alternative to river sand in construction applications. J. Clean. Prod. 205, 1114–1126. https://doi.org/10.1016/j.jclepro.2018.09.119.

Yang, R., Yu, R., Shui, Z., Gao, X., Xiao, X., Fan, D., Chen, Z., Cai, J., Li, X., He, Y., 2020. Feasibility analysis of treating recycled rock dust as an environmentally friendly alternative material in ultra-high performance concrete (UHPC). J. Clean. Prod. 258, 120673. https://doi.org/10.1016/j.jclepro.2020.120673.

Zhang, H., Ji, T., Zeng, X., Yang, Z., Lin, X., Liang, Y., 2018. Mechanical behavior of ultra-high performance concrete (UHPC) using recycled fine aggregate cured under different conditions and the mechanism based on integrated microstructural parameters. Construct. Build. Mater. 192, 489–507. https://doi.org/10.1016/j.conbuildmat.2018.10.117.

Zhang, W., Gu, X., Qiu, J., Liu, J., Zhao, Y., Li, X., 2020a. Effects of iron ore tailings on the compressive strength and permeability of ultra-high performance concrete. Construct. Build. Mater. 260, 119917. https://doi.org/10.1016/j.conbuildmat.2020.119917.

Zhang, Y., Shen, W., Wu, M., Shen, B., Li, M., Xu, G., Zhang, B., Ding, Q., Chen, X., 2020b. Experimental study on the utilization of copper tailing as micronized sand to prepare high performance concrete. Construct. Build. Mater. 244, 118312. https://doi.org/10.1016/j.conbuildmat.2020.118312.

Zhang, Z., Zhang, Zhilu, Yin, S., Yu, L., 2020c. Utilization of iron tailings sand as an environmentally friendly alternative to natural river sand in high-strength concrete: shrinkage characterization and mitigation strategies. Materials (Basel) 13, 1–15. https://doi.org/10.3390/ma13245614.

Zhao, S., Fan, J., Sun, W., 2014. Utilization of iron ore tailings as fine aggregate in ultra-high performance concrete. Construct. Build. Mater. 50, 540–548. https://doi.org/10.1016/j.conbuildmat.2013.10.019.

Zhu, Z., Li, B., Zhou, M., 2015. The influences of iron ore tailings as fine aggregate on the strength of ultra-high performance concrete. Adv. Mater. Sci. Eng. 2015 412878. https://doi.org/10.1155/2015/412878.